Effects of ion dynamics and opacity on Stark-broadened argon line profiles

D. A. Haynes, Jr., D. T. Garber, and C. F. Hooper, Jr.
Department of Physics, University of Florida, Gainesville, Florida 32611

R. C. Mancini
Department of Physics, University of Nevada, Reno, Nevada 89557

Y. T. Lee
Lawrence Livermore National Laboratory, Livermore, California 94550

D. K. Bradley, J. Delettrez, R. Epstein, and P. A. Jaanimagi
Laboratory for Laser Energetics, University of Rochester, Rochester, New York 14623
(Received 25 August 1995)

We examine the combined effects of ion dynamics and opacity on line profiles used in the analysis of hot dense plasmas. Specifically, we have calculated Stark-broadened line profiles for resonance and satellite lines of highly stripped Ar ions both in the static ion approximation and including the effects of ion dynamics. Using the results of a kinetics computer code combined with an escape factor approximation to account for the effects of radiative transfer, we have calculated the relative intensities of these lines as well as the effects of opacity on their profiles. The resulting theoretical spectrum is used in the analysis of data obtained from a series of experiments performed at the Laboratory for Laser Energetics in which plastic microballoons filled with D_2 and doped with Ar were imploded using the Omega laser system. Typical core conditions at stagnation were $n_e = 1 \times 10^{24}$ cm^{-3}, $kT = 900$ eV. Varying the relative concentration of Ar in D_2 provides an opportunity to study the combined and individual effects of ion motion and opacity on Stark-broadened line profiles.

PACS number(s): 52.70.La, 32.70.Jz

I. INTRODUCTION

X-ray emission spectroscopy has been successful in probing the hot core of laser-driven implosions [1,2]. This spectroscopy is particularly valuable as a means of diagnosing inertial confinement fusion plasmas, by means of mixing trace amounts of appropriately chosen high-Z gases into the hydrogen-isotope fuel such that, under the expected conditions of the implosion, the average dopant ion retains only a few electrons [3–7]. The amount of dopant is ideally chosen to be sufficiently small to ensure that the implosion dynamics are not appreciably effected by the dopant, but not so small as to render the diagnostic emission unobservable. Balancing these two considerations can lead to plasma compositions where a preponderance of the light fuel nuclei makes the usual static ion approximation inappropriate in the calculation of Stark-broadened line profiles. Here we will examine this issue, analyzing spectra from a series of implosion experiments where the dopant concentration was systematically altered. We will concentrate on an assessment of the individual and combined effects of ion motion and opacity on the line shape and their impact on plasma diagnostics.

In Sec. II we present the formalisms upon which we based our calculation of the temperature- and density-sensitive theoretical spectra that were used to infer plasma conditions by comparison with the experimental spectra. Time-resolved Ar emission spectra from Ar-doped implosions performed at the Laboratory for Laser Energetics at the University of Rochester are presented in Sec. III and analyzed in Sec. IV. Based on the results of this analysis, in Sec. V we will present our conclusions and suggest some areas where future work, both theoretical and experimental, might prove fruitful.

II. CALCULATION OF THEORETICAL SPECTRA

The essential idea motivating the use of Stark-broadened line profiles to diagnose hot, dense plasmas is that the line profiles themselves are strongly density dependent for the expected plasma conditions, while remaining relatively insensitive to temperature. Thus the detailed shape of the individual line profiles in the spectrum can be analyzed to yield an inference of plasma electron density. The ratios of the intensities of the lines in the spectrum are both temperature and density sensitive and, combined with the density dependence of the line shapes, can yield an inference of the plasma temperature. Our goal is to calculate temperature- and density-sensitive spectra with enough detail to model experimental data throughout the spectral region containing the Ar He-β ($1s3l \rightarrow 1s^2$), He-γ ($1s4l \rightarrow 1s^2$), He-δ ($1s5l \rightarrow 1s^2$), and Ly-β ($3l \rightarrow 1s$) lines and their attendant satellites.

As a first approximation, we model the emitting core as a sphere of uniform density and temperature ($T_i = T_e$), with a diameter consistent with mass conservation, assuming that all of the deuterium is fully stripped. The ionization state of Ar is calculated using nonlocal ther-

modynamic equilibrium (non-LTE) atomic kinetics. Future modifications of this model accounting for the existence of temperature and density gradients, motivated by the results of our analysis, will be discussed in Sec. V.

A. Stark-broadened line profiles including the effects of ion motion

In both the static [8,9] and dynamic [10] ion treatments of Stark broadening, the line shape can be written as

$$I(\omega)=\frac{4\omega^4}{3c^3}\int d\vec{\mathcal{E}}Q(\vec{\mathcal{E}})J(\omega,\vec{\mathcal{E}}) , \quad (1)$$

where $Q(\vec{\mathcal{E}})$ is the ion-microfield probability distribution function, here calculated in the adjustable parameter exponential approximation (APEX) [11]. In both cases, $J(\omega,\vec{\mathcal{E}})$ can be written

$$J(\omega,\vec{\mathcal{E}})=-\frac{1}{\pi}\,\mathrm{Im\,Tr}[\vec{d}\cdot R(\omega,\vec{\mathcal{E}})\vec{d}\rho] , \quad (2)$$

where the trace is over the relevant radiator states, $\vec{d}$ is the radiator electric dipole operator, and ρ is the density matrix of radiator states. In both the static and dynamic ion calculations, the resulting profiles are convolved with a temperature-dependent Gaussian profile to account for the Doppler effect [8,10]. For the temperatures and transitions considered here, the Doppler full width at half maximum is less than 2 eV and this effect is included in all the results presented herein. The difference between the static and dynamic theory is in the form of the resolvant $R(\omega,\vec{\mathcal{E}})$. For the dynamic case, we apply the theory of Boercker, Iglesias, and Dufty (BID) [10], in which the resolvent is approximated as

$$R(\omega,\vec{\mathcal{E}})=\frac{G(\Delta\omega,\vec{\mathcal{E}})}{1+i\nu(\Delta\omega)\int d\vec{\mathcal{E}}Q(\vec{\mathcal{E}})G(\Delta\omega,\vec{\mathcal{E}})} , \quad (3)$$

$$G(\Delta\omega,\vec{\mathcal{E}})=\frac{1}{\Delta\omega-\mathcal{L}^1_{i,r}(\vec{\mathcal{E}})-M(\Delta\omega)-i\nu(\Delta\omega)} , \quad (4)$$

where $\Delta\omega=(\omega-\omega_{\mu,\nu})\delta_{\mu\mu'}\delta_{\nu\nu'}$, $\mathcal{L}^1_{i,r}(\vec{\mathcal{E}})$ is the Liouville operator associated with the interaction of the ion microfield with the radiator's dipole, and $M(\Delta\omega)$ is the broadening tetradic due to the dynamic plasma electrons [12]. All quantities with the exception of $\nu(\Delta\omega)$ are exactly those which need to be calculated in the static ion approximation, and we use the computational methods discussed in Ref. [9].

We are left with the quantity $\nu(\Delta\omega)$. In the limit $\nu(\Delta\omega)\to 0$, we recover the result of the static ion approximation. Thus $\nu(\Delta\omega)$ is a measure of the importance of ion motion effects on the line shape. In Ref. [10] $\nu(\Delta\omega)$ is introduced as a parameter in a model for the memory operator in the evolution equation for radiator operators, fixed by the imposition of certain exact limits on the radiator momentum autocorrelation function [see Ref. [10], Eq. (2.11) and Sec. III for details]. Following BID, we approximate $\nu(\Delta\omega)$ as a real constant ν proportional to the self-diffusion coefficient for the radiator species D

$$D=\tfrac{1}{3}\int dt\,\langle\vec{v}(t)\cdot\vec{v}(0)\rangle . \quad (5)$$

The self-diffusion coefficient was calculated using a statistical mechanical model of the coupled plasma. For a fixed concentration of Ar in D_2, ν increases with increasing temperature and density. As the concentration of Ar increases, the increase in the reduced mass of the average radiator-perturbing ion pair leads to a reduction in ν and thus to a decrease in the effect of ion dynamics on the line shape.

The effect of ion dynamics is illustrated in Fig. 1, where Stark-broadened Ar He-β line shapes are displayed for fixed temperature and electron density and varying concentrations of Ar in D_2. As the concentration of Ar increases, the decreasing value of ν leads to a decreased ion-dynamic effect and thus a more marked peak structure at or near line center. Changing the concentration of Ar in D_2 also modifies $Q(\vec{\mathcal{E}})$, which primarily effects the wings and the separation between the peaks. The effects of ion dynamics are responsible for the large effect on the dip at line center. In general, the effect of ion dynamics is to broaden the line around the peaks, within one ion plasma frequency of each of the peaks. For lines with a sizeable central dip, e.g., the β lines, the effect of ion dynamics is most obvious as a filling in of the dip. The effect of ion dynamics decreases with increasing Ar concentration, with the 100% Ar case most resembling the static result.

B. Opacity broadening

Having calculated the Stark-broadened line shapes including the effects of ion motion, it is necessary to include other effects before making comparisons with the experimental data. In the optically thin approximation, the intrinsic line shape (calculated as above) would be simply convolved with an instrumental response function. However, as the concentration of Ar increases we need to account for opacity effects as well. The effects of opacity broadening, like those of ion dynamics, are most obvious near the peaks of the line shape, though, unlike the effect of ion dynamics, opacity can also distort the wings. At the peaks, the redistribution of photons is most readily

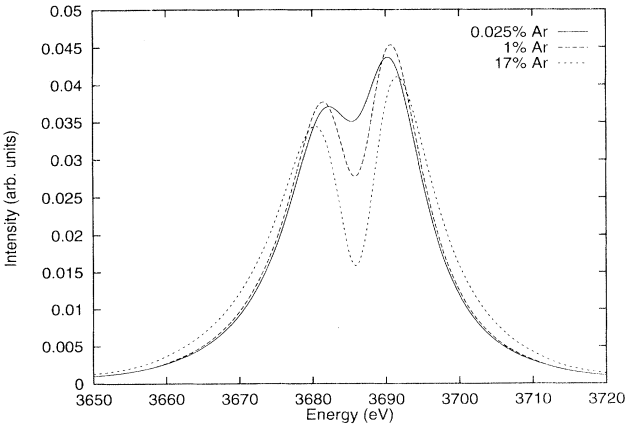

FIG. 1. Area-normalized dynamic Stark-broadened Ar He-β line shapes, calculated for 0.025% ($\nu=3.37$ eV), 1% ($\nu=1.66$ eV), and 17% Ar in D_2 ($\nu=0.621$ eV); $n_e=5\times10^{23}$ cm^{-3} and $kT=900$ eV.

apparent, as photons from the peaks of the line are redistributed into the wings where they have a better chance of escaping and being detected. For the small concentrations of Ar in D_2 we will approximate opacity broadening using a modified slab opacity formula [13]. In this approximation, prior to convolution with instrumental response function, the area-normalized observed line shape is given by

$$I_{\rm obs}(\omega)=A(1-e^{-\tau_\omega}) , \tag{6}$$

where A is a normalization constant and τ_ω, the frequency-dependent optical depth, is given by

$$\tau_\omega=\frac{\pi e^2}{mc}\hat{f}\hat{I}(\omega)N_l d , \tag{7}$$

where $\bar{f}$ is the effective oscillator strength for the transition of interest, the circumflex denotes area normalization with respect to the frequency variable $\omega/2\pi$, N_l is the number density of ions in the lower states of the transition, and d is the average chord length in the plasma. In Fig. 2 we display the opacity broadening on the line shape, comparing the Ar He-β line calculated in the optically thin, static ion approximation with the calculations that include first opacity and then both opacity and ion dynamics. When both ion dynamics and opacity effects are included, there is a corresponding decrease in the calculated optical depth at line peak τ_0: τ_0, which was 0.66 for the static ion calculation in Fig. 2, is reduced to 0.59 when the calculation includes ion dynamic effects. The peak structure of the observed line shape is effected by both opacity broadening and ion motion and the response of these two effects to changes in Ar concentration is competitive. Care must be taken to account for both effects in line shapes calculated for the purpose of analyzing experimental data.

C. Non-LTE relative intensities and radiative transfer effect

Having calculated the line shapes for the individual transitions of interest, we must now combine them with the correct relative intensities to form our theoretical spectrum. A non-LTE kinetic model [14] was used to calculate the relative intensities of the lines in the model spectrum. The model includes all the ionization stages in Ar from P-like Ar (Ar^{+3}) to the fully stripped ion (Ar^{+18}). For each ionization stage, the model includes the ground-state configuration and several excited-state configurations. The amount of detail in the model is greatest in the Li-, He-, and H-like stages and doubly excited states are treated self-consistently with ground and singly excited states. In particular, for Li-like Ar the model includes 918 energy levels, with sufficient detail to calculate the populations for the upper states of the Li-like satellites of the He-β line with spectator electrons in $n=2$, 3, and 4. For the plasma conditions of interest, the relative distribution of population within the $1s2l3l'$ or the $1s3l3l'$ doubly excited states is close to LTE, while the populations of these two manifolds are not in LTE with respect to each other, nor are they in LTE with the upper state of the He-β line. It is therefore important to do the non-LTE modeling to make a realistic estimate of the relative intensities of the satellite lines to their associated resonance lines. An important temperature dependence in our model is in the ratio of the Ly-β intensity to the He-β intensity since they correspond to different ionization stages. This strong dependence constrains our temperature inferences. Also, the ratios of the intensities of the Li-like satellites to the He-β line are considerably temperature sensitive and, for a given electron density, there is a narrow temperature range where both the intensity of the Ly-β line and these satellites are comparable; thus the simultaneous observation of these features is a useful temperature diagnostic in itself.

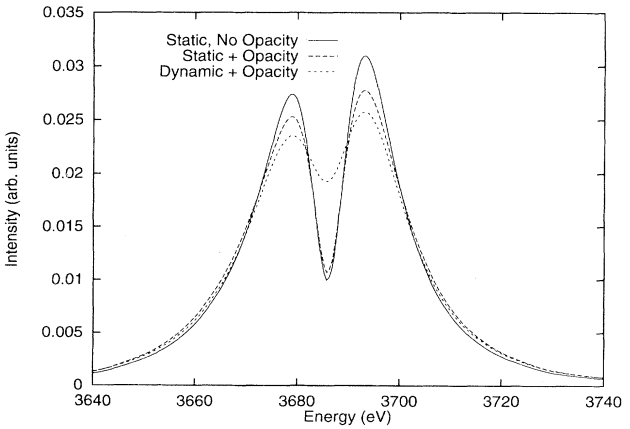

FIG. 2. Ion dynamics and opacity effects on the area normalized Ar He-β line shape, for $n_e=10\times10^{23}$ cm^{-3}, $kT=900$ eV, 0.25% Ar in D_2, and diameter $=25$ μm.

The non-LTE kinetics calculations were performed in the steady-state, optically thin approximation, as we are most interested in analyzing plasmas with low concentrations of Ar, for which the ion motion effects on the line shapes will be most noticeable. While at first glance these optically thin calculations seem reasonable, given the small fraction of Ar in D_2 for the plasmas of interest, they lead to a substantial underestimation of the intensity of the Ly-β line. The transfer of the optically thick ($\tau_0\sim10$) He-α line from the core leads to a shift in the ionization balance towards higher ionization stages, which results in a decrease of He-like Ar and an increase in H-like Ar. We estimated this effect on the resonance lines in our model using an escape factor approximation [15]. To this end, escape factors for the He-α, He-β, He-γ, and He-δ line transitions in He-like Ar and Ly-α, Ly-β, and Ly-γ in H-like Ar were calculated using Stark-broadened line profiles for several electron densities n_e, assuming a uniform and spherical plasma, following the method described in Ref. [15]. As an illustration of these results, escape factors for the He-β line are displayed in Fig. 3 as a function of $X=\tau_\omega/\phi(\omega)=\tau_0/\phi_0=(\pi e^2/mc)fN_lR$, where R is the radius of the plasma sphere. The use of Stark-broadened line profiles results in escape factors that are n_e dependent through the line shapes (besides the dependence through τ_0): as the electron density n_e increases, changes in the line profiles (larger width, stronger wings) result in an increase in the

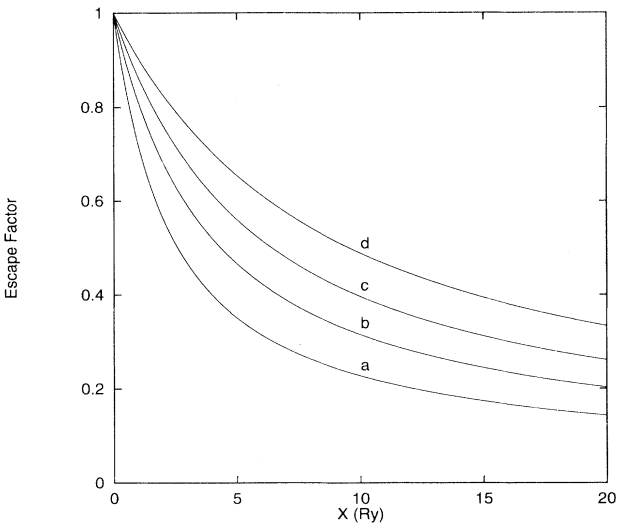

FIG. 3. Escape factors for the He-β line vs $X=\tau_\omega/\phi(\omega)=\tau_0/\phi_0$ for several values of the electron density N_e: (a) 2×10^{23} cm^{-3} ($\phi_0=0.2454$ Ry^{-1}), (b) 5×10^{23} cm^{-3} ($\phi_0=0.1392$ Ry^{-1}), (c) 1×10^{24} cm^{-3} ($\phi_0=0.1041$ Ry^{-1}), and (d) 2×10^{24} cm^{-3} ($\phi_0=0.0826$ Ry^{-1}).

escape factor values. These escape factors were used in the atomic kinetics calculations to account for opacity effects; they affect the computation of excited level populations as well as the total emergent line intensity.

The inclusion of this effect leads to model spectra, which can fit simultaneously the relative intensities of the resonance lines as well as the relative intensities of the resonance lines to their attendant satellites. Thus, while opacity has a small impact on the individual line shapes, it is important in determining the relative intensities. The effect of radiative transfer on the resonance line intensities in our model is shown in Table I for two different Ar concentrations. In this table we list C, the correction to the ratio of intensities due to radiative transfer, defined for line x as

$$C_x=\frac{\left[\frac{I_x}{I_{\mathrm{Ly}-\beta}}\right]_{\mathrm{thick}}}{\left[\frac{I_x}{I_{\mathrm{Ly}-\beta}}\right]_{\mathrm{thin}}}, \tag{8}$$

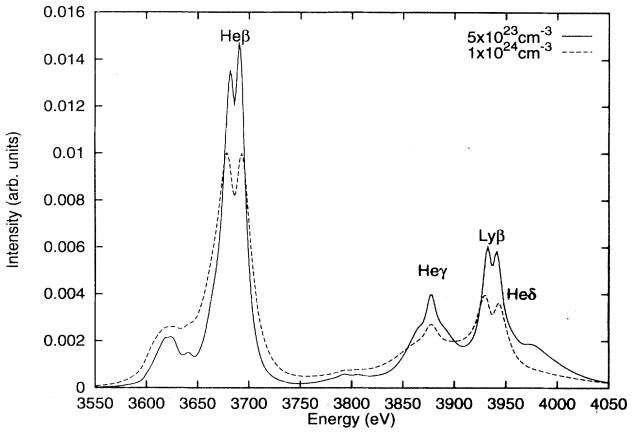

FIG. 4. Density sensitivity of the model spectrum, for $kT=900$ eV and 0.25% Ar in D_2. The centers of gravity of the Ar resonance lines included in our model are indicted.

where I_x is the integrated intensity of line x, and "thick" and "thin" denote the results of the optically thick and thin non-LTE models, respectively.

The sensitivity of our model spectrum to changes in density and temperature is indicated in Figs. 4 and 5. The positions of the centers of gravity of the Ar resonance lines are indicated in Fig. 4. Included in our model are five satellites to these resonance lines: the Li-like satellites of the Ar He-β line with the spectator electron in $n=2$ (center of gravity 3623 eV) and $n=3$ (3669 eV), the He-like satellites of the Ar Ly-β line with the spectator electron in $n=2$ (3871 eV) and $n=3$ (3918 eV), and the Li-like satellite of the Ar He-γ line with the spectator electron in $n=2$ (3797 eV). Our model spectrum shows sufficient temperature and density sensitivity to be useful in the analysis of plasmas whose electron temperatures range from 600 to 1200 eV and whose electron densities lie between 5 and 20×10^{23} cm^{-3}.

III. EXPERIMENTAL DATA

A series of laser-driven implosions was conducted at the Laboratory for Laser Energetics at the University of Rochester. The series was designed, in part, to explore the inter-relationship between spectral line broadening

TABLE I. Radiative transfer corrections to the ratios of the integrated intensities of the He-like resonance lines in the model to the integrated intensity of the Ar Ly-β, for $n_e=8\times10^{23}$ cm^{-3}, and different number concentrations of Ar in D_2 and temperatures. Diameters: 27 μm (0.25% Ar) and 28 μm (1% Ar).

kT_e	$C_{\mathrm{He}-\beta}$		$C_{\mathrm{He}-\gamma}$		$C_{\mathrm{He}-\delta}$	
(eV)	0.25% Ar	1% Ar	0.25% Ar	1% Ar	0.25% Ar	1% Ar
500	0.76	0.42	0.89	0.67	0.91	0.73
600	0.59	0.29	0.71	0.48	0.74	0.53
700	0.50	0.27	0.60	0.43	0.62	0.48
800	0.48	0.29	0.56	0.44	0.57	0.48
900	0.49	0.34	0.55	0.48	0.56	0.51
1000	0.51	0.40	0.56	0.52	0.57	0.55
1100	0.54	0.45	0.58	0.56	0.58	0.58
1200	0.56	0.50	0.59	0.59	0.60	0.61

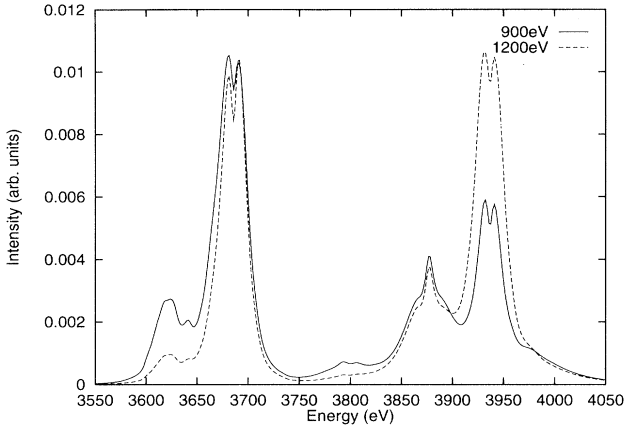

FIG. 5. Temperature sensitivity of the model spectrum, for $n_e = 5 \times 10^{23}$ cm^{-3} and 1% Ar in D_2.

due to dynamic ions and that due to opacity in Ar K-shell spectra. The targets were 250-μm-diam plastic microballons filled with 20 atm of Ar and D_2 in varying concentrations, ranging from 0.025% Ar to pure Ar. The wide range of Ar concentrations was chosen so that the transition from ion-dynamic-dominated peaks to opacity dominated peaks could be studied. Core conditions at stagnation were such that K-shell Ar line emission was easily observable. Time-resolved spectra were recorded using a flat-crystal spectrograph (FCS). The FCS has an ammonium dihydrogen phosphate crystal with a two-dimensional spacing of 10.642 Å coupled to an x-ray streak detector. The instrument response is detector limited, i.e., streak camera resolution. With a target to detector distance of 300 mm, the source size broadening is negligible.

We will discuss here the data from five shots, taken from the high-resolution FCS data. In all five shots, the FCS was imaging the spectral region from around 3400–4200 eV, where the Ar He-β, He-γ, and He-δ, and Ly-β lines, along with their attendant satellites, are located. The instrumental response function is approximated by a Gaussian, whose full width at half maximum is energy dependent, ranging from 3.6 eV at 3680 eV to 4.4 eV at 3935 eV.

The lowest concentration of Ar in D_2 in this series of experiments was 0.01 atm of Ar in 20 atm of D_2, a number concentration of 0.025% Ar. In this shot, the attempt to observe diagnostically useful Ar line emission was unsuccessful.

With ten times as much Ar as in the previous target, the implosion with 0.25% Ar in D_2 (which we will designate A) yielded the useful time-dependent spectra, which we display in Fig. 6. The five lineouts show each average over approximately 50 ps, while the time intervals over which the lineouts are averaged overlap by 25 ps with the neighboring lineouts.

The two shots with 0.4 atm of Ar in 19.6 atm D_2 (a concentration of 1% Ar in D_2) produced enough signal such that the window over which the time integration was done could be shrunk to 25 ps, with no overlap. Figure 7 shows the time-resolved spectra from one of these shots, designated B.

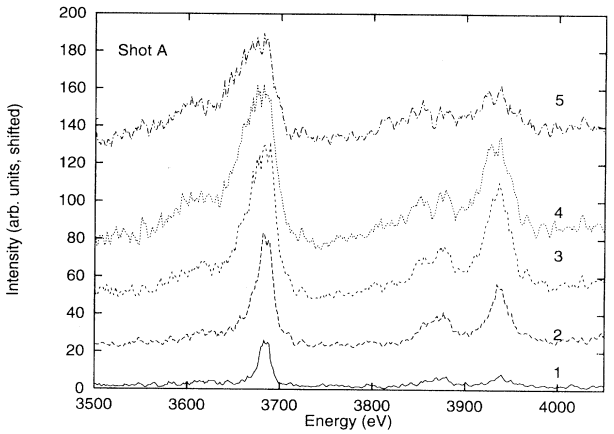

FIG. 6. Time-resolved lineouts from shot A (0.25% Ar in D_2). Labels used in the text refer to individual lineouts. Individual lineouts are shifted vertically by an arbitrary amount for display purposes. The five lineouts shown each average over approximately 50 ps and the time intervals over which they average overlap by 25 ps with neighboring lineouts.

With 5 atm of Ar in D_2 (17% Ar in D_2), the last implosion we consider here did not achieve high enough temperatures to produce useful Ar emission spectra in our range of interest possibly due to a combination of the increased target mass and radiative cooling.

IV. ANALYSIS

We now use our model spectrum to analyze the data from the shots designated A and B. We will concentrate on two aspects of the analysis. First, we will focus on the He-β line and its Li-like satellites. The temperature and density sensitivity of this composite feature has been presented previously, in the static-ion optically thin ap-

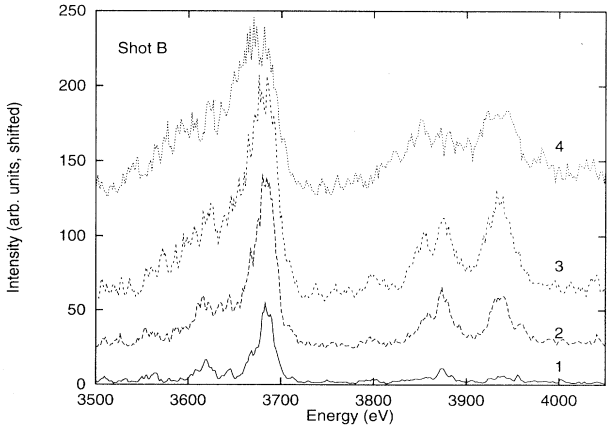

FIG. 7. Time-resolved lineouts from shot B (1% Ar in D_2). Labels used in the text refer to individual lineouts. Individual lineouts are shifted vertically by an arbitrary amount for display purposes. The four lineouts shown each average over approximately 25 ps, with no overlap between consecutive time intervals.

proximation [16,17]. This composite spectral feature, the most prominent feature in all the spectra we consider, best illustrates the importance of both ion dynamics and opacity broadening on the line shape. Second, we will illustrate the utility of our model spectrum by attempting to fit the spectral region from 3500 to 4100 eV for a lineout from shot *B*. Preliminary results from the use of our model spectrum, absent the effects of radiative transfer on the intensity ratios, have been presented previously [18]. We will consider the consistency of our fits throughout this spectral region and test the accuracy of our temperature and density inferences. Before comparison, the model spectrum was convolved with our approximation to the instrumental response function and a background was subtracted from the experimental spectrum. The model spectrum was shifted arbitrarily by between 1 and 5 eV in the direction of lower energy to match the locations of the lines in the experimental data.

The role that ion dynamics plays in the formation of the line emission spectra for low concentrations of Ar in D_2 is indicated in Fig. 8, where the He-β + Li-like satellites composite spectrum from lineout 3 of shot *A* (0.25% Ar in D_2) is compared to our model calculation. In Fig. 8(a) the effect of opacity on the line shape is seen to be minimal, as the small concentration of Ar prevents significant redistribution of intensity. However, for this low concentration of Ar in D_2, opacity alone cannot account for the lack of a central dip in the observed He-β line. When the effect of ion dynamics is included [Fig. 8(b)], the dip in our model spectrum is commensurate with the experimental data. Analyses of other lineouts from this shot also indicate that opacity alone cannot explain the lack of a large central dip in the He-β line, while the inclusion of ion dynamic effects in the line-shape calculation leads to spectra that compare well with the experimental data.

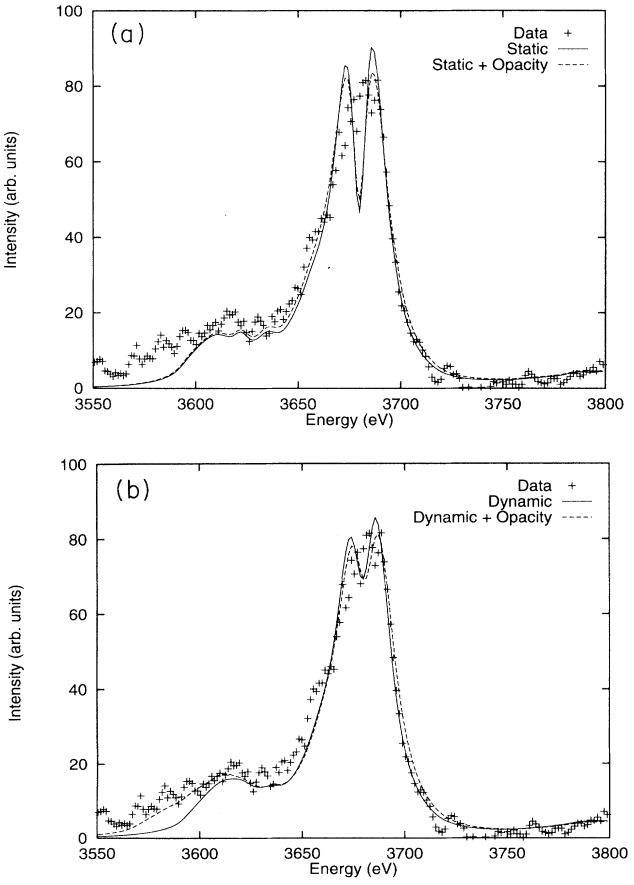

FIG. 8. Detail from lineout *A*-3 (0.25% Ar in D_2) and fits using model spectrum, for $n_e = 8\times10^{23}$ cm^{-3} and $kT = 925$ eV. Only the fit labeled "Dynamic + Opacity" includes the correction for satellite emission in the (3550–3600)-eV region, as discussed in the text.

The first three fits in Fig. 8 (Static, Static + Opacity, and Dynamic) indicate a deficiency in our model spectrum. Our model predicts negligible emission in the region from 3550 to 3600 eV, on the red side of the $n=2$ Li-like satellite of the He-β line. As the Li-like satellites obviously contribute to the emission on the red side of the He-β line, it is natural to consider the importance of Be-like satellites in the spectral region where our model is deficient. There are transitions in this region in Be-like Ar from the $1s2l2l'3l''$ manifold to the $1s^2 2l2l'$ mainfold. Though our kinetic model did not include sufficient detail in the Be-like ionization stage to calculate the intensity of this line, we can include it in our model spectrum with its intensity of a free parameter. Such an inclusion is justified by data from similar shots where the FCS was imaging the α lines of Ar. In those shots, the emission from the Be-like satellite of the He-α line is apparent. The final fit in Fig. 8 (Dynamic + Opacity) includes an estimate of the intensity from the Be-like satellite, as a preliminary attempt to assess the importance of emission from this satellite.

Shot *B*, with four times the Ar concentration of shot *A*, allows us to explore the importance of ion dynamics on the line shape when opacity is not negligible. Figure 9 is similar to Fig. 8 in that it compares our model spectra to the He-β + Li-like satellites composite spectral feature from the data. As the concentration of Ar in D_2 increases, the effect of opacity on the line shape becomes more important and ion dynamics has less of an effect on the peak structure. Indeed the density inference from this lineout depends on the inclusion of opacity, as the effect of opacity, while most noticeable on the peak structure, is also important for the overall line shape.

In Fig. 9 there is a noticeable discrepancy between our calculated spectrum and the experimental data, in the spectral region around 3640 eV. There is emission in this region in the data that is not present in our model. While this is the most blatant occurrence of this discrepancy, other lineouts also display greater intensity in this region than our calculations predict. The unaccounted for emission occurs in the location of the blue peak of the $n=2$ Li-like satellite of the He-β line. The discrepancy is greatest for low-density conditions, occurring early in the implosions. We conjecture that non-LTE or time-dependent effects or level mixing among the initial manifolds of the Li-like satellites not included in our model may enhance the emission in this region.

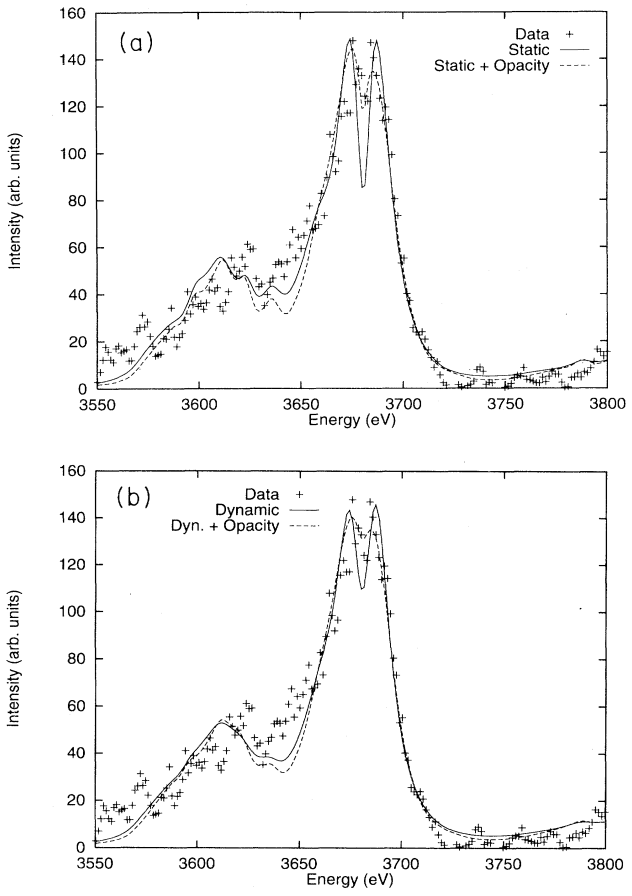

FIG. 9. Detail from lineout *B*-3 (1% Ar in D_2) and fits using model spectrum. Static, $n_e = 8\times10^{23}$ cm^{-3} and $kT = 875$ eV; Static + Opacity, $n_e = 5\times10^{23}$ cm^{-3} and $kT = 840$ eV; Dynamic, $n_e = 8\times10^{23}$ cm^{-3} and $kT = 875$ eV; Dynamic + Opacity, $n_e = 5\times10^{23}$ cm^{-3} and $kT = 840$ eV.

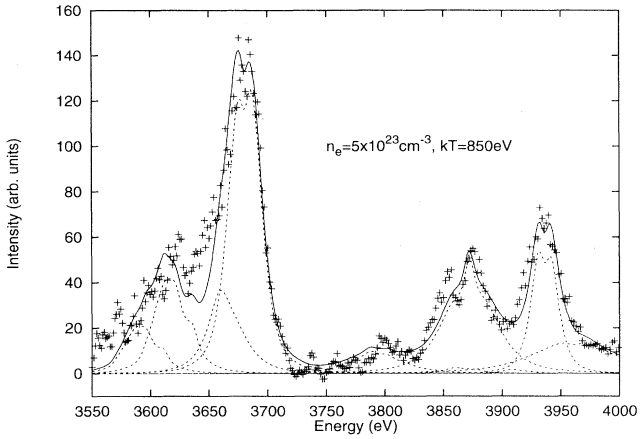

FIG. 10. Best fit to lineout *B*-3 (1% Ar in D_2), for $n_e = 5\times10^{23}$ cm^{-3} and $kT = 850$ eV. The dashed traces are the individual line profiles that were added to produce the model spectrum.

Having explored the importance of ion dynamics and opacity on the line shape, we turn to an examination of the utility of our model spectra as a tool for the inference of plasma temperature and density. We model line emission from the spectral region 3550–4000 eV, including in our calculation the Ar Ly-β line and its He-like satellites with the spectator electron in $n = 2$ and 3, the Ar He-β and its Li-like satellites with the spectator in $n = 2$ and 3, the He-γ line and its $n = 2$ Li-like satellite, and the He-δ line. We account for Be-like emission around 3580 eV in the manner indicated before.

The density inference is most easily made by fitting the blue wings of the He-β and the Ly-β line. These wings are less effected by the presence of satellites than the red wings, though care must be taken to include the He-δ line

TABLE II. Inferences of plasma conditions obtained by comparing model spectra with the experimental data of Figs. 8 and 9, over the spectral range 3550–4000 eV.

Lineout	Density (10^{23} cm^{-3})	Temperature (eV)	Diameter (μm)
	Shot *A* 0.25% Ar in D_2		
1	<5[a]		
2	5	1000	32
3	8	1050	27
4	10	1025	25
5	10[b]	950	25
	Shot *B* 1% Ar in D_2		
1	$\ll 5$[a]		
2	<5[c]		
3	5	850	33
4	8	880	28

[a]The early lineouts come from times when the electron density was less than 5×10^{23} cm^{-3}, the lowest electron density we considered when preparing our model spectrum.

[b]The fit at 10×10^{23} cm^{-3} indicates that the electron density is slightly higher.

[c]Although this lineout is remarkably well fit with a optically thin model spectrum with an electron density of 5×10^{23} cm^{-3} and electron temperature of 800 eV, the amount of opacity that we calculate for the lines at these conditions is appreciable and leads to lines that are overly broad. This is another illustration of the importance of the inclusion of opacity effects on the line shape for even this small concentration of Ar in D_2.

when considering the blue side of the Ly-β line. These wings display enough density sensitivity to distinguish between lines emitted from plasmas whose densities differ by a factor of 1.5 in this regime of plasma conditions. Thus we can distinguish between emission from lineouts characteristic of 5, 8, and 10×10^{23} cm^{-3}.

Given a density inference, we can inquire about the average temperature of the emitting region. In Fig. 10 we fit the entire spectral region from 3550 to 4000 eV for the third lineout from shot *B*. The temperature inferences from this fit is within 10% of those obtained by separately fitting the region containing only the He-β line and its Li-like satellites and the region containing only the Ly-β, He-γ, and He-δ lines, and their satellites. This degree of consistency is typical of our results for this type of test. This accuracy in temperature inference can be attributed to the strong constraints put on the fit in that it has to reproduce emission emanating from transitions in three different ionization stages in Ar. Indeed, it was just this constraint that led to our appreciation of the importance of the radiative transfer effect on the intensity of the Ly-β line relative to the intensities of the other lines in the model. Without the inclusion of this effect, it proved impossible to fit the intensity of the Li-like satellites of the He-β and Ly-β lines simultaneously with a single temperature. The density and temperature inferences obtained from our analysis of shots *A* and *B* are presented in Table II.

V. CONCLUSION

From the preceding analysis, it is clear that a model combining the intertwined effects of ion dynamics and opacity is required for consistent fitting of the spectral data from implosions where a small amount of Ar is added to the fuel for diagnostic purposes. For the 0.25% Ar case, the effect of ion dynamics on the line shape was necessary to model the peaks in the experimental data. If we use static line shapes to fit the data for this case, one would infer optical depths and thus plasma diameters that are too large by a factor of 2 to be consistent with the diameters measured by x-ray microscopes [18]. For the 1% Ar case, the effect of opacity on the line shape was more important to fit the peaks in the data, though the effects of ion dynamics were not negligible. Also, in both cases the radiative transfer effect on the relative intensities of these lines is important in providing consistent relative intensities for the resonance lines and their satellites.

While the results presented here do show the importance of ion dynamics on the Ar line shapes emitted from deuterium plasmas doped with trace amounts of argon, the resolution of the experimental data near the peaks of the resonance lines is not sufficient to distinguish between differing theories of ion dynamics. Higher-resolution spectroscopy of, say, the He-β line would go far in testing the detailed effect of ion dynamics on the line shape and the results presented here point to plasma compositions and conditions where such experiments could be carried out fruitfully. Currently, a detailed comparison of the results of the method used here to include ion dynamic effects in the calculation of Stark-broadened line shapes with results of a different method [19] is underway. Another advantage of higher-resolution spectroscopy would be the ability to probe the effects of the real part of $M(\Delta\omega)$, both on the location and shapes of the lines [12].

Our model spectrum is calculated assuming that the radiating region of the plasma can be characterized by a single temperature and density. While the model spectrum produced using this assumption is capable of reproducing many of the features of the experimental data, some aspects of the fits, particularly in the region around the peak of the He-γ line, are unsatisfactory. Work is in progress to assess the importance of gradients. Preliminary studies modeling radiation from a layered core structure appear promising.

[1] H. R. Griem, Phys. Fluids B **4**, 2346 (1992).
[2] C. F. Hooper, Jr., R. C. Mancini, D. A. Haynes, Jr., and D. T. Garber, in *Elementary Processes in Dense Plasmas,* edited by S. Ichimaru and S. Ogata (Addison-Wesley, Reading, MA, 1995).
[3] H. Nishimura *et al.*, Phys. Plasmas **2**, 2063 (1995).
[4] T. R. Dittrich *et al.*, Phys. Rev. Lett. **73**, 2324 (1994).
[5] C. J. Keane, B. A. Hammel, A. Osterheld, and D. R. Kania, Phys. Rev. Lett. **72**, 3029 (1994).
[6] B. A. Hammel *et al.*, J. Quant. Spectrosc. Radiat. Transfer **51**, 113 (1994).
[7] A. Hauer *et al.*, Phys. Rev. A **28**, 963 (1983), which contains references to earlier experiments, and in which both non-LTE and gradient effects are considered.
[8] L. A.Woltz and C. F. Hooper, Jr., Phys. Rev. A **8**, 4766 (1988).
[9] R. C. Mancini, D. P. Kilcrease, L. A. Woltz, and C. F. Hooper, Jr., Comput. Phys. Commun. **63**, 314 (1991).
[10] D. B. Boercker, C. A. Iglesias, and J. W. Dufty, Phys. Rev. A **36**, 2254 (1987).
[11] C. A. Iglesias, J. L. Lebowitz, and D. A. MacGowan, Phys. Rev. A **28**, 1667 (1983).
[12] Only the imaginary part of $M(\Delta\omega)$, that part leading to electron broadening is included in our calculation. Although shifts due to the radiator-plasma electron interaction have received considerable theoretical attention [see, e.g., H. R. Griem *et al.*, Phys. Rev. A **41**, 5600 (1990); M. Koenig *et al.*, *ibid.* **38**, 2089 (1988); J. Cooper in *Radiative Properties of Hot Dense Matter,* edited by J. Davis *et al.* (World Scientific, Singapore, 1985)], we have found no compelling experimental evidence in our data of overall shifts due to this interaction, nor of additional modification of the line shape due to differential shifting of individual components. Thus we have not yet included this part of the radiator-plasma electron interaction in our calculations.
[13] N. D. Delamater *et al.*, Phys. Rev. A **31**, 2460 (1985).
[14] Y. T. Lee, J. Quant. Spectrosc. Radiat. Transfer **38**, 131

(1987).

[15] R. C. Mancini, R. F. Joyce, and C. F. Hooper, Jr., J. Phys. B **20**, 2975 (1987). A comparison of the radiative transfer effect as calculated in the escape factor approximation and in the solution of the linearized transfer equation can be found in C. J. Keane *et al.*, J. Quant. Spectrosc. Radiat. Transfer **54**, 207 (1995).

[16] R. C. Mancini *et al.*, Rev. Sci. Instrum. **63**, 5119 (1992).

[17] C. Keane *et al.*, Phys. Fluids B **5**, 3328 (1993).

[18] D. A. Haynes *et al.*, Rev. Sci. Instrum. **66**, 755 (1995).

[19] A. Calisti *et al.*, J. Quant. Spectrosc. Radiat. Transfer **51**, 59 (1994).